

Flow Law, Microstructure and Corrosion Behavior of Friction Stir Welded 5A06 Alloy

Li Yajie, Qin Fengming, Liu Cuirong, Wu Zhisheng

Taiyuan University of Science and Technology, Taiyuan 030024, China

Abstract: The evolution of metal flow, microstructure and corrosion properties of 5A06 alloy after friction stir welding were studied. Results show that the metal on the advancing side is curled directly into the threads and then is extruded down into the weld nugget zone by complex motions of torsion and swirl. However, the material on the retreating side encounters chaotic flow patterns. The electro backscattering diffraction results indicate that the grains in stir zone are pronouncedly refined by dynamic recrystallization, and the average grain size is about 6 μm . The scanning electron microscope analyses display that β -phase (Al_3Mg_2) and $\text{Al}_6(\text{Mn}, \text{Fe})$ are dispersedly distributed in the stir zone and the $\text{Al}_6(\text{Mn}, \text{Fe})$ is smaller than that in base material. The hardness profile is characterized by material softening along the cross-section and the minimum hardness (HV) value of 720 MPa is located in the interface between stirring zone and thermo-mechanically affected zone. It is evident that the stir zone exhibits better corrosion resistance than the base material. The corrosion potential of stir zone is 35 mV larger than that in base material (-0.725 V).

Key words: aluminum alloy; friction stir welding; flow pattern; microstructure; corrosion behavior

Due to the growing demand for reduction of exhaust gas emission in shipbuilding, aerospace and transportation industries, aluminum alloys with light weight have been used to gradually replace the conventional structural materials^[1-3]. 5xxx Al-Mg alloy, characterized by the higher strength-to-weight ratio, anti-corrosion performance and high hardness, offers great potential for weight saving in shipbuilding. However, it is well known that the welding of aluminum alloys using conventional fusion welding methods will cause a series of severe issues like porosity, high residual stress and many cracks, which severely limited the industrial application of aluminum alloys^[4]. Thus it is very important to explore the better welding methods for the joining of aluminum alloys.

The innovative friction stir welding (FSW) is a solid state joining technique with a larger number of promising advantages for welding Al alloys^[5-9]. The equipment of FSW consisting of rotating shoulder and pin, is relatively simple. During the welding process, the non-consumable rotating pin is inserted into the sheets with proper tilt angle and then moves to the direction of the welding line. By the combination

of tool rotation and linear motion, the sheets are joined without fusion. During friction stir welding process, the material undergoes severe plastic deformation and thermal exposure, which induce complicated metal flow and microstructure evolution. The past several decades witnessed a lot of studies on the friction stir welding of 2xxx and 7xxx aluminum alloy, while fewer investigations on the friction stir welding of 5xxx aluminum alloy. In particular, relatively little attention was paid to delineate the flow pattern and the microstructure evolution of the 5A06 alloy via friction stir welding.

The object of this study is to reveal the details of the flow pattern, microstructure evolution and the microstructure-property relationships during friction stir welding of Al-Mg alloy. Therefore, the 5A06 alloys produced by friction stir welding were examined by the electron back-scatter diffraction (EBSD) technique. Moreover, in order to study the corrosion performance of the aluminum alloy welds, the immersion test and electrochemical corrosion test were employed to provide in-depth insight about the correlation

Received date: October 12, 2017

Foundation item: National Natural Science Foundation of China (51275332)

Corresponding author: Wu Zhisheng, Ph. D., Professor, School of Materials Science and Engineering, Taiyuan University of Science and Technology, Taiyuan 030024, P. R. China, E-mail: zswu@tyust.edu.cn

Copyright © 2018, Northwest Institute for Nonferrous Metal Research. Published by Elsevier BV. All rights reserved.

between precipitates and corrosion performance of the welds.

1 Experiment

The materials used in the present study were as-extruded commercial 5A06 aluminum alloy with the thickness of 12 mm. The base material (BM) was with a nominal chemical composition of 5.8 wt% Mg, 0.5 wt% Mn, 0.14 wt% Fe, 0.065 wt% Cu, 0.043 wt% Si, 0.04 wt% Zn, 0.04 wt% Ti and balance Al. After polished by abrasive paper and cleaned with ethanol, butt joints were welded along the extruding direction by a simple FSW tool fabricated from H13 steel with a shoulder and a cone threaded pin. The schematic illustration of FSW is shown in Fig.1. Through a lot of experiments, it was found that a defect free joint was obtained at the preferable welding parameters, i.e. the welding speed of 80 mm/min and the rotation rate of 220 r/min. During friction stir welding process, the pin tool was tilted by 3° from the sheet normal and rotated in a clockwise direction. The principal directions of the joints are denoted as normal direction (ND), welding direction (WD) and transverse direction (TD).

The welded samples were sectioned perpendicular to the welding direction. The microstructures of the material before and after FSW were studied by optical microscopy (OM), X-ray diffraction (XRD) and EBSD technique. The sectioned samples were etched with mixture reagent (1 mL HF, 1.5 mL HCl, 2.5 mL HNO₃ and 95 mL H₂O) for OM observation. The samples for EBSD were ground on SiC paper of 3000# grit and then electropolished in 10 vol% perchloric acid plus 90 vol% alcohol solution at 10 V for 15 s at room temperature. The EBSD testing was performed on a ZEISS ULTRA 55 field-emission scanning electron microscopy with a step size of 0.8 μm . The HKL Channel 5 software was used to analyze the EBSD scan data.

Vickers microhardness test was carried out across the cross-section perpendicular to the welding direction, using a load of 2 N and a dwell time of 15 s for each indent. The corrosive medium used in the present study was 3.5 wt% NaCl solution. The samples for immersion and electrochemical test were cut from base material and top nugget with exposure area of 1 cm² by an electric-sparking wire-cutting machine. The samples for immersion test were ground to 3000# grit and then immersed in 3.5 wt% NaCl solution for 72 h at temperature of 25 °C. After the immersion test, the samples were cleaned in chromic acid consisting of 200 g/L CrO₃. Then the corrosion behavior of samples after immersion was analyzed by scanning electron microscope (SEM). Electrochemical tests were conducted in 3.5 wt% NaCl solution at 25 °C using a classical three-electrode cell (the sample with an exposed area of 1 cm² as working electrode, platinum wire as counter electrode and a saturated calomel electrode as reference electrode) after the open circuit potential reached stability.

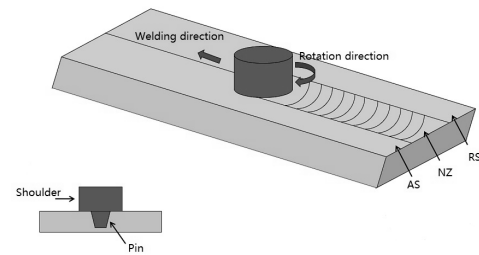


Fig.1 Schematic illustration of FSW

2 Results and Discussion

2.1 Material flow

A low-magnification overview of the cross-section of friction stir weld is shown in Fig.2. The retreating side (RS) and advancing side (AS) correspond to the left-hand and right-hand, respectively. The heat affected zone (HAZ), thermo-mechanically affected zone (TMAZ), stir zone (SZ) and crown zone (CZ) are delineated using black lines on the basis of optical microstructure. No porosity and cracks are produced in the weld, which indicates that the aluminum alloy is well welded by friction stir welding with welding speed of 80 mm/min and rotation rate of 220 r/min. A large number of banded structures are mainly observed in the SZ close to the advancing side, which indicates that the plastic deformation of weld is asymmetrical and material flow in the advancing side is much more severe than that in the retreating sides. Those partially developed banded structure mainly located in the advancing side have been reported by Tao et al^[10]. In addition, similar to the previous studies^[10-12], lazy S or kissing bond defects can be distinctly observed in the stir zone with the lower rotation rate of 220 r/min, which is mainly due to the relatively high deformation resistance of the 5xxx aluminum.

Fig.2 shows inhomogeneous macrostructures in different zones of weld indicating plastic deformation during friction stir welding process are chaotic, as reported by previous investigations^[7,13-15]. In this section, in order to reveal the material flow pattern during friction stir welding process in more details, typical feature of different regions marked in Fig.2 are displayed in Fig.3. Fig.3a ~3d are the optical images in the stir

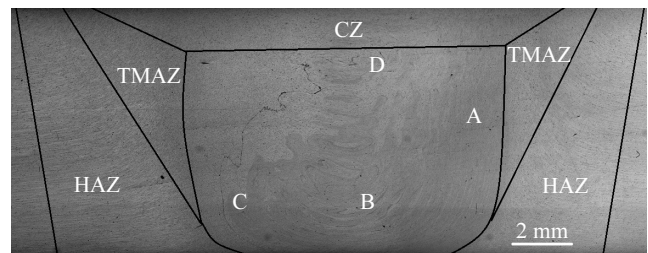


Fig.2 Optical image of the cross-section of friction stir welded 5A06 alloy

zone close to advancing side (region A marked in Fig.2), on the bottom of the stir zone (region B), in the MID-SZ close to retreating side (region C) and in the upper part of stir zone (region D), respectively.

Fig.3a reveals that the materials around position A distinctly move downward into the weld nugget zone. It is very possible that the material on the advancing side of the weld is curled directly into the threads of the rotational pin tool and then is extruded down into the stir zone by complex motions of torsion and swirl. This suggests that threaded pin can move some material from the upper part of the weld to deeper into the weld, which is in line with the study reported by Colligan and Donatus^[16,17]. Fig.3b displays a change in flow direction from downward flow to horizontal flow (from AS to RS). This typical flow may be attributed to a simple extrusion process. It is well known that the plastic metal is moved in a closed area consisting of shoulder, blacking plate and un-plasticized base material. As the flow metal (around region A) is pushed into the bottom of the stir, it will be restricted by the closed area and be moved into the zone close to retreating side. However, the material around region C encounters chaotic flow, as displayed in Fig.3c. It may be attributable to complex combinations of extrusion force (from thread) and resistance (from blacking plate). That is to say, the downward force in retreating side may be less than that in advancing side, which lead to complex flow in RS while single vertical flow in AS. Fig.3d displays the obvious horizontal flow pattern in the upper section of the weld. Compared with the material on bottom of the weld, the flow material around region D is located in the shoulder domain zone. Therefore, this horizontal flow is associated with the torsion produced by the rotational shoulder. The material on the upper section of the weld is pulled from

RS to AS and eventually end up in the rear of the rotational pin tool, which is in good agreement with the previous study^[18]. Another interesting point is that the position of lazy S defects also indicates the distinct material flow patterns in different zone of the weld, as shown in Fig.2. On the bottom of the weld, the lazy S defects are restricted to the zone near the RS resulting from the horizontal flow from AS to RS. On the upper section, however, lazy S defects are pushed into the AS indicating the horizontal flow from RS to AS. Based on these observations, we can draw a conclusion that not all the material encounters the rotational motion, but the material in some zones may experience simple extrusion motion, which result in the complex metal flow in the weld after friction stir welding.

2.2 Microstructure analysis

The characteristic microstructural feature of as-extruded base material is shown in Fig.4a. It consists of substantial coarse grains and a small fraction of relatively fine grains. The average grain size is about 28 μm based on the linear intercept method. A few coarse grains are located in the direction perpendicular to the extrusion force. The microstructure of TMAZ close to the base material is characterized by the flattened and elongated grains, as shown in Fig.4b, which is attributed to the vertical compression from the shoulder tool. Fig.4c shows that there is a difference in grain size between base material and stir zone. The average grain size of SZ is about 6 μm . The fine equiaxed grains are formed through the dynamic recrystallization during the friction stir welding process, which has been reported by previous studies^[8,19-21]. It is very possible that the temperature, mainly produced by the friction action between the shoulder tool and plate, is higher than the dynamic recrystallization temperature of Al alloy, so that the original coarse grains are completely replaced by the

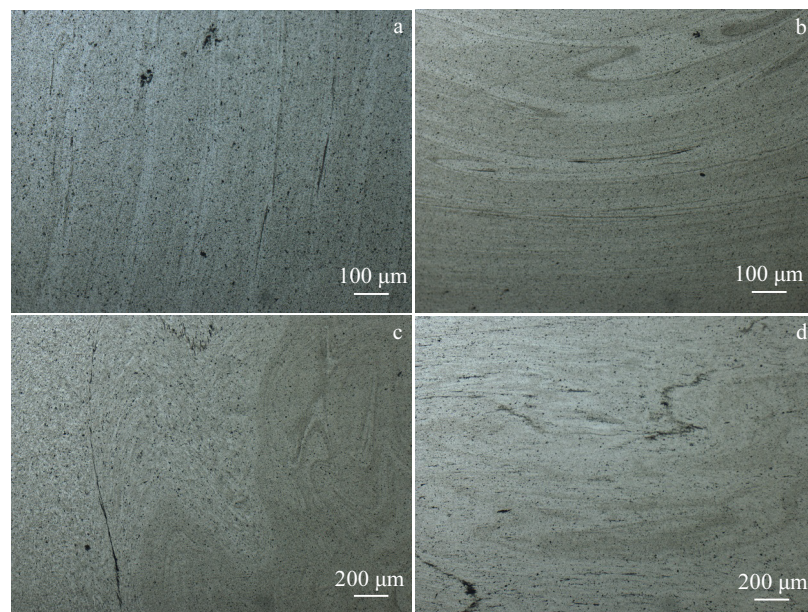


Fig.3 Typical feature of different regions marked by A (a), B (b), C (c) and D (d) in Fig.2

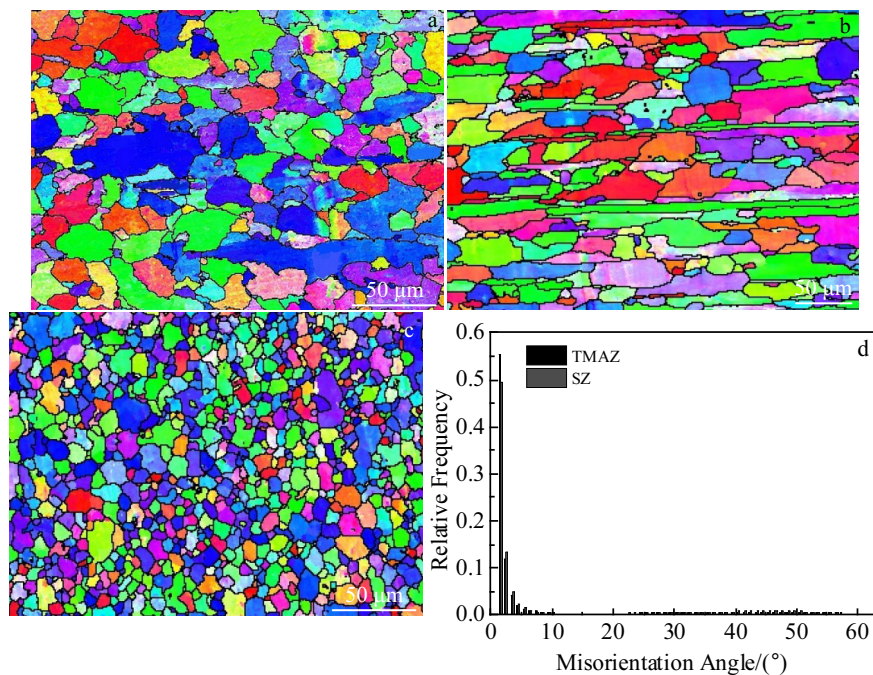


Fig.4 EBSD maps in different zones of FSWed weld: (a) base material, (b) TMAZ close to the base material, and (c) SZ; (d) grain boundary misorientation distribution plot

recrystallized grains in the SZ. In addition, compared to the TMAZ, the low angle boundary fraction of SZ decreases while the high angle boundary fraction increases, as shown in Fig.4d. It indicates that the dynamic recrystallization in SZ exerts a significant influence on the increasing of the high angle boundary fraction via consuming the low angle boundary.

Some second phases are observed in the base metal, TMAZ

and SZ of the weld as displayed in Fig.5. There are two main typical precipitates in the base material (Fig.5a). Polygon-like precipitates containing the elements Al, Fe and Mn, aggregate into clusters. The EDS analysis of point 1 in Fig.5a is shown in Fig.5d. Thus, these second phases presumably are $Al_6(Mn, Fe)$ which are the main precipitates in 5xxx aluminum alloy reported by previous studies^[22-24]. Of particular interest is the

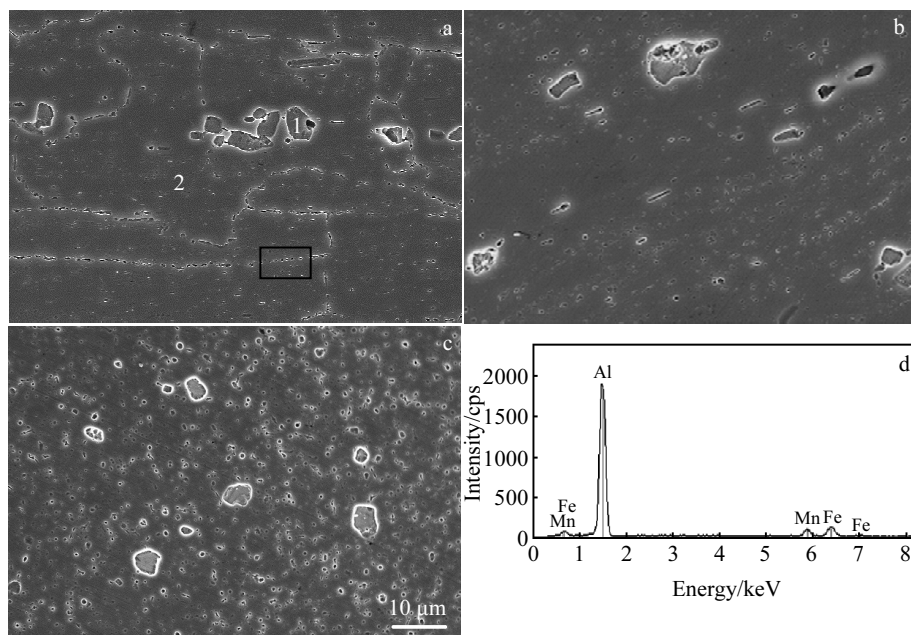


Fig.5 SEM micrographs of the different regions in weld: (a) BM, (b) TMAZ close to SZ, and (c) SZ; (d) EDS spectrum of point 1 marked in Fig.5a

observation in Fig.5a that a thin layer of second phases with the size less than 1 μm is precipitated along grain boundaries. Zhu et al. have reported that Mg tend to form precipitates (Al_3Mg_2) with the size in nano-scale along the grain boundaries^[25]. Thus, it is very possible that these precipitates in the grain boundaries are β -phase Al_3Mg_2 . The XRD analysis of the base material and SZ are shown in Fig.6. The test results indicate that the material in two conditions are mainly composed of phases α -Al, β -phase (Al_3Mg_2) and $\text{Al}_6(\text{Mn, Fe})$, which is in line with the results of SEM and EDS. However, the distribution of those precipitates in TMAZ and SZ is different from the base material compared with the Fig.5a~5c. The β -phase (Al_3Mg_2) and $\text{Al}_6(\text{Mn, Fe})$ are dispersedly distribute d in the SZ and the $\text{Al}_6(\text{Mn, Fe})$ is smaller than that in base material, which is due to the crushing force produced by the rotational pin tool. The distribution of these second phases is in accordance with the direction of metal flow in TMAZ.

2.3 Hardness analysis

Fig.7 shows the hardness profile at the mid-thickness line of the cross-section of 5A06 alloy from the weld center to the base material. It should be emphasized that the hardness measurement is conducted after natural aging for 100 d. The hardness of SZ is distinctly higher than that of the TMAZ. This is partly due to the smaller grains in SZ, which can be

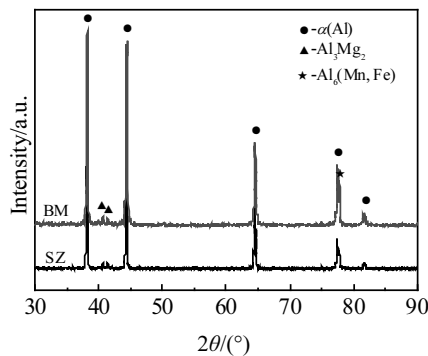


Fig.6 XRD patterns of the 5A06 alloy before and after FSW process

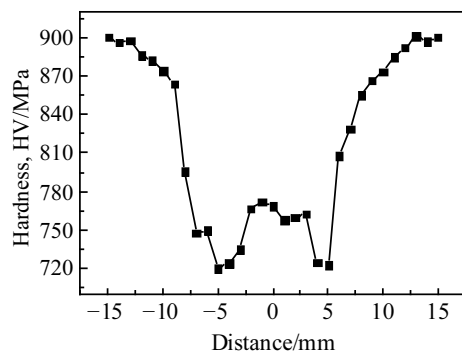


Fig.7 Microhardness profile of the weld

well demonstrated by Hall-Petch relationship^[26,27]. It is very possible that fine-grained SZ has a greater total grain boundary area which can represent barriers and severely impede the dislocation action. In addition, the reprecipitation of the hardening phase during natural aging process also increases the hardness of the SZ^[28]. Another interesting point is the observation that micro-hardness profile is characterized by pronounced softening of material along the weld. The minimum value of micro-hardness (720 MPa) is located in the interface between SZ and TMAZ, which is also reported by previous investigations^[29].

2.4 Corrosion analysis

The detailed corrosion behavior was studied by immersion tests in 3.5 wt% NaCl solution. The surface morphologies of the BM and SZ for 72 h are shown in Fig.8. It can be seen that the corrosion is more severe in the case of the BM than the SZ (Fig.8a and Fig.8c). Moreover, it should be emphasized that the corrosion mainly originates from the matrix close to the $\text{Al}_6(\text{Mn, Fe})$, as shown in Fig.8b and Fig.8d. Due to the higher corrosion potential of the $\text{Al}_6(\text{Mn, Fe})$ than α -Al^[30], the corrosion rate of the matrix close to these precipitates is accelerated. Thus, taking into account more flocculent $\text{Al}_6(\text{Mn, Fe})$ precipitates in BM than that in SZ, the occurrence of the more severe corrosion in base material should be expected. In addition, after the friction stir welding, the concentration level of the $\text{Al}_6(\text{Mn, Fe})$ decreases, which also improves the corrosion resistance of the SZ. That is to say, the difference of corrosion resistance is associated with the distribution and size of precipitates, which is consistent with the reported investigation of the Al alloys^[31,32]. The β -phase (Al_3Mg_2) also affects the corrosion resistance of the Al alloys. However, the corrosion behavior of this second phase can't be observed by SEM, so that this work will be dealt with in further investigations.

In attempting to further analyze the corrosion rate of base material and SZ, electrochemical tests were done at a constant scanning rate of 0.5 mV/s after an initial delay of 2000 s. Fig.9a shows the potentiodynamic polarization curves for the two alloys in 3.5 wt% NaCl solution. The corrosion potential, E_{corr} , of the base material is -0.725 V, while that of SZ is about 35 mV more positive. By making intersection points of the tangents of the upper and below portion of potentiodynamic polarization curves, the corresponding corrosion current density (i_{corr}) is obtained. It reveals that SZ has the lower i_{corr} than BM^[33]. It is very possible that the galvanic effect between aluminum alloy matrix and $\text{Al}_6(\text{Mn, Fe})$ precipitates is associated with quantities, distribution and size of the $\text{Al}_6(\text{Mn, Fe})$ precipitates. $\text{Al}_6(\text{Mn, Fe})$ is more evenly distributed in SZ than that in BM resulting in higher corrosion potential and lower corrosion current density in SZ. In addition, XRD results show that the quantities of Al_3Mg_2 in BM are higher than those in SZ, as shown in Fig.6. It indicates that some Al_3Mg_2 are dissolved into the Al matrix resulting from stir action and thermal exposure. It is well known that the corrosion

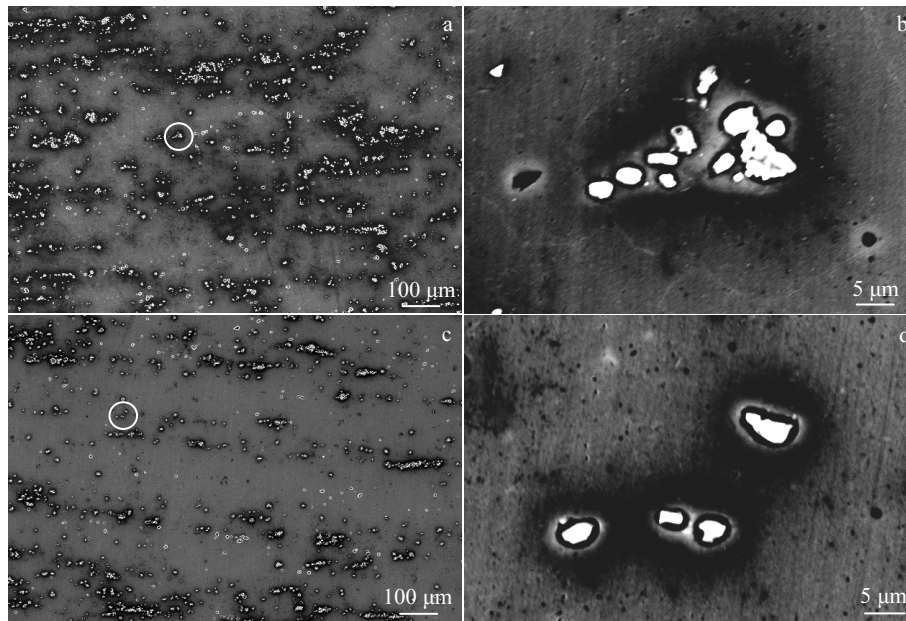


Fig.8 SEM images of the corroded surface of the BM (a, b) and SZ (c, d) after 72 h exposure in the 3.5 wt% NaCl solution

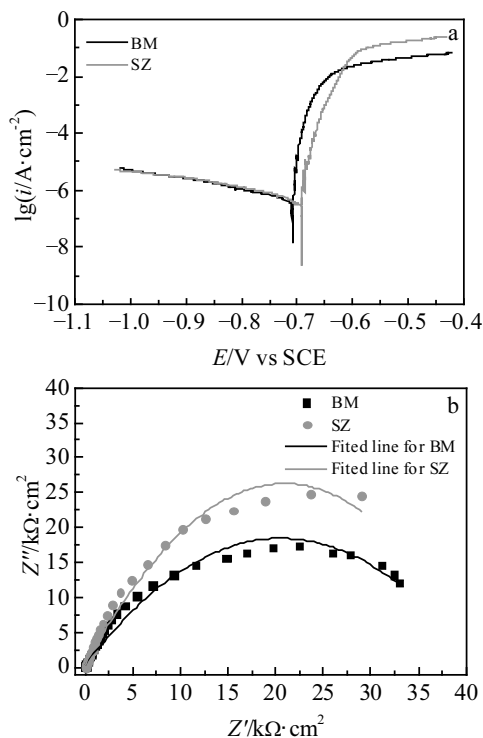


Fig.9 Potentiodynamic polarization curves (a) and Nyquist plots (b) of the sample before and after FSW process

potential of Al_3Mg_2 is -1.29 V which is about 560 mV more negative than that of the $\alpha\text{-Al}$ (0.73 V). That is to say, the dissolution of the Al_3Mg_2 can provide an inhibiting electrochemical effect which increases corrosion resistance of

SZ. The Nyquist plots of the two samples are displayed in Fig.9b. It can be seen that the diameter of the loop for SZ is much larger than that of BM, which also demonstrates that BM is more susceptible to the corrosion than SZ.

3 Conclusions

1) On the advancing side, the friction stir welded 5A06 alloy is curled directly into the threads and then is extruded down into the weld nugget zone by complex motions of torsion and swirl. However, on the retreating side, the metal encounters chaotic flow patterns due to complex combinations of extrusion force (from thread) and resistance (from blanking plate).

2) The grain size in SZ is about five times less than that in BM. The grain refinement in SZ is mainly due to dynamic recrystallization activated by rotational action of pin tool and thermal exposure.

3) β -phase (Al_3Mg_2) and $\text{Al}_6(\text{Mn}, \text{Fe})$ are dispersedly distributed in SZ resulting from the severe stirring movement. The quantities of Al_3Mg_2 also obviously decrease after FSW.

4) The hardness of the joint is lower than that of the base material, and the minimum value of hardness is located in the SZ/TMAZ interface. In addition, the stir zone exhibits better corrosion resistance than the base material.

References

- 1 Dursun T, Soutis C. *Materials and Design*[J], 2014, 56: 862
- 2 Gibson B T, Lammlein D H, Prater T J et al. *Journal of Manufacturing Processes*[J], 2014, 16(1): 56
- 3 Menzemer C, Srivatsan T S. *Materials Science and Engineering A*[J], 1999, 271(1-2): 188

- 4 Guo N, Fu Y L, Wang Y Z et al. *Materials and Design*[J], 2017, 113: 273
- 5 Gabrielli F, Forcellese A, El Mehtedi M et al. *Procedia Engineering*[J], 2017, 183: 245
- 6 Sudhagar S, Sakthivel M, Mathew P J et al. *Measurement*[J], 2017, 108: 1
- 7 Seidel T U, Reynolds A P. *Metallurgical and Materials Transactions A*[J], 2001, 32(11): 2879
- 8 Martinez N, Kumar N, Mishra R S et al. *Journal of Alloys and Compounds*[J], 2017, 713: 51
- 9 Peng Y Y, Yin Z M, Lei X F et al. *Rare Metal Materials & Engineering*[J], 2011, 40(2): 201
- 10 Tao Y, Zhang Z, Ni D R et al. *Materials Science and Engineering A*[J], 2014, 612: 236
- 11 Delrue S, Tabatabaeipour M, Hettler J et al. *Ultrasonics*[J], 2016, 68: 71
- 12 Kadlec M, Růžek R, Nováková L. *International Journal of Fatigue*[J], 2015, 74: 7
- 13 Guerra M, Schmidt C, McClure J C et al. *Materials Characterization*[J], 2002, 49(2): 95
- 14 Prangnell P B, Heason C P. *Acta Materialia*[J], 2005, 53(11): 3179
- 15 Ouyang J H, Kovacevic R. *Journal of Materials Engineering and Performance*[J], 2002, 11(1): 51
- 16 Colligan B K. *Welding Research*[J], 1999, 172: 229
- 17 Donatus U, Thompson G E, Zhou X et al. *Materials and Design*[J], 2015, 83: 203
- 18 Pashazadeh H, Teimournezhad J, Masoumi A. *Materials and Design*[J], 2014, 55: 619
- 19 Cam G, Mistikoglu S. *Journal of Materials Engineering and Performance*[J], 2014, 23(6): 1936
- 20 Abdulstaar M A, Al-Fadhalah K J, Wagner L. *Materials Characterization*[J], 2017, 126: 64
- 21 Tan Y B, Wang X M, Ma M et al. *Materials Characterization*[J], 2017, 127: 41
- 22 Engler O, Miller-Jupp S. *Journal of Alloys and Compounds*[J], 2016, 689: 998
- 23 Liu P, Li Y, Zhang G M et al. *Vacuum*[J], 2016, 131: 65
- 24 Aziz I, Zhang Q, Xiang M. *Chinese Journal of Aeronautics*[J], 2009, 22(6): 670
- 25 Zhu Y K, Cullen D A, Kar S et al. *Metallurgical and Materials Transactions A*[J], 2012, 43(13): 4933
- 26 Park S H C, Sato Y S, Kokawa H. *Journal of Materials Science*[J], 2003, 38(21): 4379
- 27 Chang C I, Lee C J, Huang J C. *Scripta Materialia*[J], 2004, 51(6): 509
- 28 Feng A H, Chen D L, Ma Z Y. *Metallurgical and Materials Transactions A*[J], 2010, 41(4): 957
- 29 Chen J, Fujii H, Sun Y F et al. *Materials Science and Engineering A*[J], 2012, 549: 176
- 30 Tan L, Allen T R. *Corrosion Science*[J], 2010, 52(2): 548
- 31 Li S, Dong H G, Shi L et al. *Corrosion Science*[J], 2017, 123: 243
- 32 Liu S G, Ren P Y, Wang G Y et al. *Royal Society of Chemistry*[J], 2015, 6: 320
- 33 Peng Y, Shen C B, Zhao Y D et al. *Rare Metal Materials & Engineering*[J], 2017, 46(2): 344

5A06 铝合金搅拌摩擦焊接接头的金属流动规律、显微组织以及腐蚀行为

李亚杰, 秦凤明, 刘翠荣, 吴志生

(太原科技大学, 山西 太原 030024)

摘要: 对 5A06 铝合金在搅拌摩擦焊接过程中的金属流动规律以及焊后显微组织演变和腐蚀行为进行研究。结果表明: 由于受到扭转和漩涡运动的综合作用, 前进侧金属被直接卷入搅拌针的螺纹内部, 然后被向下挤压进入焊核区。然而, 后退侧的金属展现出无序的金属流动模式。通过扫描电子显微镜电子背散射分析发现, 搅拌区的晶粒在动态再结晶的作用下发生了明显的细化, 再结晶后平均晶粒尺寸约为 6 μm 。对搅拌区的扫描电子显微分析结果表明, β 相(Al_3Mg_2)和 $\text{Al}_6(\text{Mn}, \text{Fe})$ 呈弥散分布, 且和母材相比 $\text{Al}_6(\text{Mn}, \text{Fe})$ 颗粒明显细化。同时, 焊缝截面的硬度分布表明焊后 5A06 铝合金具有软化趋势, 最小硬度值 (HV) 为 720 MPa, 位于搅拌区和热机影响区的界面处。通过电化学分析和浸泡后的组织观察发现搅拌区的耐腐蚀性明显优于母材, 母材的腐蚀电位为 -0.725 V , 而搅拌区域腐蚀电位升高 35 mV。
关键词: 铝合金; 摩擦搅拌焊; 流动模式; 显微组织; 腐蚀行为

作者简介: 李亚杰, 男, 1985 年生, 博士, 太原科技大学材料科学与工程学院, 山西 太原 030024, E-mail: liyajie1207@126.com